JACS
JOURNAL OF THE AMERICAN CHEMICAL SOCIETY

ARTICLE

pubs.acs.org/JACS

Large Endohedral Fullerenes Containing Two Metal Ions, $Sm_2@D_2(35)$-C_{88}, $Sm_2@C_1(21)$-C_{90}, and $Sm_2@D_3(85)$-C_{92}, and Their Relationship to Endohedral Fullerenes Containing Two Gadolinium Ions

Hua Yang,[†] Hongxiao Jin,[†] Bo Hong,[†] Ziyang Liu,*[,†] Christine M. Beavers,[‡] Hongyu Zhen,[§] Zhimin Wang,[§] Brandon Q. Mercado,[∥] Marilyn M. Olmstead,*[,∥] and Alan L. Balch*[,∥]

[†]College of Materials Science and Engineering, China Jiliang University, Hangzhou 310027, China

[‡]Advanced Light Source, Lawrence Berkeley National Lab, One Cyclotron Road, Berkeley, California 94720, United States

[§]State Key Laboratory of Modern Optical Instrumentation and Department of Chemistry, Zhejiang University, Hangzhou 310027, China

[∥]Department of Chemistry, University of California, One Shields Avenue, Davis, California 95616, United States

Supporting Information

ABSTRACT: The carbon soot obtained by electric arc vaporization of carbon rods doped with Sm_2O_3 contains a series of monometallic endohedral fullerenes, $Sm@C_{2n}$, along with smaller quantities of the dimetallic endohedrals $Sm_2@C_{2n}$ with n = 44, 45, 46, and the previously described $Sm_2@D_{3d}(822)$-C_{104}. The compounds $Sm_2@C_{2n}$ with n = 44, 45, 46 were purified by high pressure liquid chromatography on several different columns. For endohedral fullerenes that contain two metal atoms, there are two structural possibilities: a normal dimetallofullerene, $M_2@C_{2n}$, or a metal carbide, $M_2(\mu\text{-}C_2)@C_{2n-2}$. For structural analysis, the individual $Sm_2@C_{2n}$ endohedral fullerenes were cocrystallized with Ni(octaethylporphyrin), and the products were examined by single-crystal X-ray diffraction. These data identified the three new endohedrals as normal dimetallofullerenes and not as carbides: $Sm_2@D_2(35)$-C_{88}, $Sm_2@C_1(21)$-C_{90}, and $Sm_2@D_3(85)$-C_{92}. All four of the known $Sm_2@C_{2n}$ endohedral fullerenes have cages that obey the isolated pentagon rule (IPR). As the cage size expands in this series, so do the distances between the variously disordered samarium atoms. Since the UV/vis/NIR spectra of $Sm_2@D_2(35)$-C_{88} and $Sm_2@C_1(21)$-C_{90} are very similar to those of Gd_2C_{90} and Gd_2C_{92}, we conclude that Gd_2C_{90} and Gd_2C_{92} are the carbides $Gd_2(\mu\text{-}C_2)@D_2(35)$-$C_{88}$ and $Gd_2(\mu\text{-}C_2)@C_1(21)$-$C_{90}$, respectively.

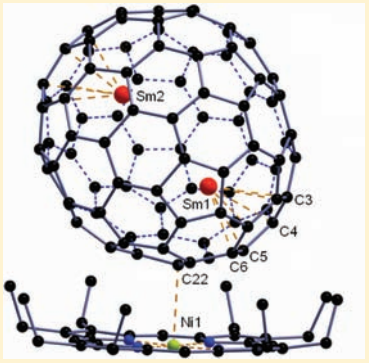

INTRODUCTION

While C_{60} and C_{70} are the most abundant and well-known fullerenes, endohedral metallofullerenes,[1,2] which consist of a closed carbon cage with one or more metal atoms trapped inside, represent a related class of molecules whose properties can be altered by changing the nature and number of the metal atoms inside. Thus, endohedral fullerenes containing gadolinium have been shown to be effective as relaxation agents for use in magnetic resonance imaging (MRI)[3,4] and may be instrumental in developing new types of MRI contrast agents that effectively encapsulate the potentially hazerdous gadolinium ions.[5] Likewise, endohedral fullerenes containing lutetium atoms have potential as X-ray imaging agents due to the high absorptivity of the encapsulated Lu.[6]

Generally, the fullerene cages that encapsulate metal atoms are larger than C_{60}. Numerous endohedral fullerenes involving carbon cages in the C_{74}−C_{84} range have been structurally identified by single-crystal X-ray diffraction,[7,8] but far fewer X-ray crystal structures are available for endohedral fullerenes with larger carbon cages. Nevertheless, a number of endohedrals with larger cage sizes have been reported. For example, a series of soluble digadolinium endohedrals that extends from Gd_2C_{90} to Gd_2C_{124} has been detected in the carbon soot produced by the Krätschmer−Huffman electric arc method of fullerene formation with graphite rods filled with Gd_2O_3.[9]

For endohedral fullerenes that contain two metal atoms such as the Gd_2C_{90}−Gd_2C_{124} series, there are two structural possibilities. The compound may exist as a normal dimetallofullerene, $M_2@C_{2n}$, or the compound may involve a metal carbide and have the formula, $M_2(\mu\text{-}C_2)@C_{2n-2}$. Well-characterized examples of the normal dimetallofullerene, $M_2@C_{2n}$, class that have been isolated and structurally characterized include: the IPR obeying endohedrals $Er_2@C_s(6)$-C_{82},[10] $Er_2@C_{3v}(8)$-C_{82},[11] $La_2@I_h$-C_{80},[12] $M_2@D_{3h}$-C_{78} (M = Ce,[13] La[14]), and $M_2@D_2(10611)$-C_{72} (M = La[15] or Ce[16]) and the non-IPR $La_2@C_2(10611)$-C_{72}.[17] Examples of the metal carbide class include: $Sc_2(\mu\text{-}C_2)@C_{68}$,[18] $Sc_2(\mu\text{-}C_2)@C_{2v}(5)$-$C_{80}$,[19] the three isomers of $M_2(\mu\text{-}C_2)@C_{82}$

Received: July 6, 2011
Published: September 14, 2011

dx.doi.org/10.1021/ja206244w | J. Am. Chem. Soc. 2011, 133, 16911–16919

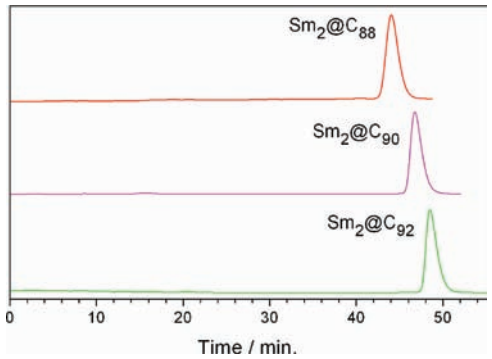

Figure 1. Chromatograms of the isolated $Sm_2@C_{2n}$ (n = 44−46) isomers on a Buckyprep column with toluene as the eluent. The HPLC conditions are flow rate of 4.0 mL/min and detection wavelength of 450 nm.

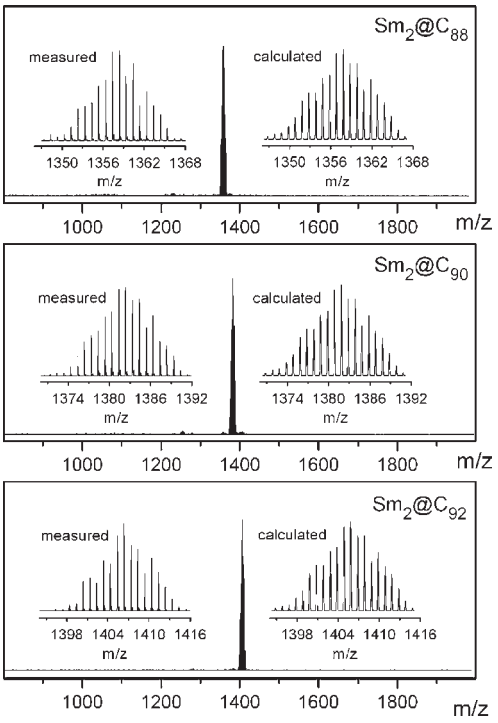

Figure 2. LDI-TOF mass spectra of the purified samples of $Sm_2@C_{2n}$ (n = 44−46). The insets show expansions of the measured and calculated isotope distributions.

(M = Sc, Y) with different fullerene cage geometries (C_s, C_{2v}, and C_{3v}) that were characterized by ^{13}C NMR spectroscopy,[20] and $Sc_2(\mu\text{-}C_2)@D_{2d}\text{-}C_{84}$.[3] One of the two isolated isomers of Gd_2C_{94} has been shown by X-ray crystallography to have the carbide structure, $Gd_2(\mu\text{-}C_2)@D_3(85)\text{-}C_{92}$.[9] In this carbide, the $Gd_2(\mu\text{-}C_2)$ unit has a butterfly shape with the $(\mu\text{-}C_2)$ unit perpendicular to a line drawn between the two Gd atoms.

The nanocapsule, $Sm_2@D_{3d}(822)\text{-}C_{104}$, is the largest dimetallofullerene to be structurally characterized to date.[21] This fact is somewhat surprising, because samarium-containing endohedral fullerenes are generally produced in lower yields than found for other lanthanum metals.[22] Previous papers have reported the formation of an extensive series of monosamarium containing endohedrals that run from $Sm@C_{74}$ to $Sm@C_{96}$,[23−25] but these articles did not report the observation of any disamarium endohedrals.

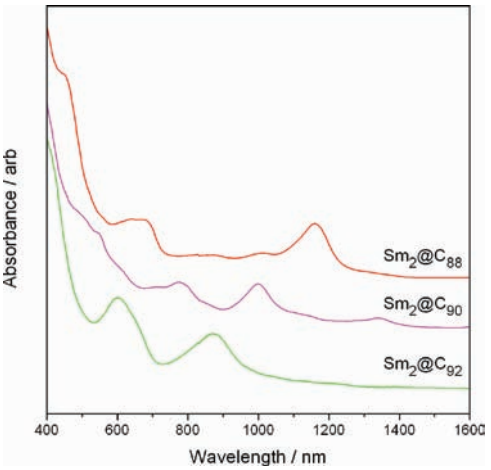

Figure 3. UV/vis/NIR absorption spectra of the isolated $Sm_2@C_{2n}$ (n = 44−46) endohedral fullerenes dissolved in carbon disulfide.

Here, we report the isolation and structural characterization of three new disamarium endohedrals and compare their properties with the corresponding digadolinium endohedrals. In making comparisons between endohedrals containing these two metals, it is important to note that gadolinium belongs to the class of metals that transfer three electrons to the carbon cage and is present as Gd^{3+} when encapsulated, while samarium is one of the lanthanides that transfers only two electrons to the fullerene cage and is present as Sm^{2+}.[26]

RESULTS AND DISCUSSION

Isolation and Characterization of $Sm_2@C_{2n}$ Endohedral Fullerenes. Carbon soot containing the samarium endohedral fullerenes along with empty cage fullerenes was obtained by vaporizing a graphite rod filled with Sm_2O_3 and graphite powder in an electric arc as outlined earlier.[18,27] The soot was extracted with *o*-dichlorobenzene and concentrated. This soluble extract was subjected to a four-stage, high performance pressure liquid chromatographic (HPLC) isolation process that resulted in the separation and successful characterization by X-ray crystallography of four Sm_2C_{2n} species with n = 44, 45, 46, and 52. Figure 1 shows the chromatograms of the three new endohedrals that were isolated, and Figure 2 shows their laser-desorption ionization time-of-flight (LDI-TOF) mass spectra. The UV−vis−NIR absorption spectra of the individual endohedrals are shown in Figure 3.

While procedures for the isolation of these three new Sm_2C_{2n} species have been found, it is important to note that these compounds are found in much smaller amounts than are the series of monosamarium endohederals, $Sm@C_{74}$ to $Sm@C_{96}$, reported earlier.[21−23] Thus, under similar conditions, the formation of Sm-containing endohedrals differs significantly from the formation of Gd-containing endohedrals.[9] With samarium, the formation of $Sm@C_{2n}$ dominates over the formation of Sm_2C_{2n} species, while with gadolinium the formation of Gd_2C_{2n} endohedrals is the major process. Only a few monogadolinium endohedrals ($Gd@C_{60}$,[28] $Gd@C_{82}$[29,30]) have been reported.

Single-Crystal X-ray Diffraction Studies of the Three New $Sm_2@C_{2n}$ Endohedral Fullerenes. All of the fullerenes were cocrystallized with Ni(OEP) to aid crystal growth and structure refinement, as previously described.[31] Crystallographic analysis

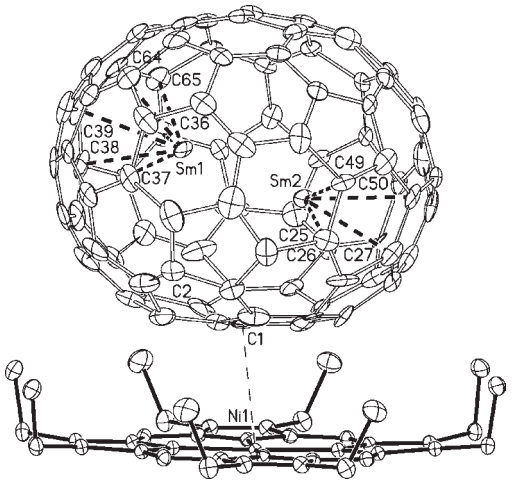

Figure 4. A portion of the structure of $Sm_2@D_2(35)$-C_{88}·Ni(OEP)·2toluene showing 35% probability displacement ellipsoids for non-hydrogen atoms. Only the major sites (74% occupancy) for the fullerene and for the Sm atoms (54% for Sm1 and Sm2) are shown. For clarity, the hydrogen atoms and toluene molecules are omitted. The Sm---Sm distance shown is 4.216(3) Å. The range of Sm···C distances is 2.51−2.66 Å.

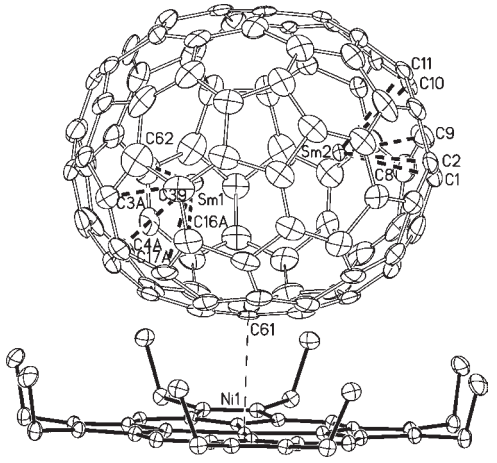

Figure 5. A portion of the structure of $Sm_2@C_1(21)$-C_{90}·Ni(OEP)·2toluene showing the major cage orientation (66% occupancy) and major Sm sites (64% occupancy for Sm1, 43% for Sm2) with 35% probability displacement ellipsoids for non-hydrogen atoms. The toluene molecules are omitted. The Sm---Sm distance shown is 4.1459(10) Å. The range of Sm···C distances is 2.33−2.72 Å.

has resulted in the structural identification of three of the dimetal endohedrals as $Sm_2@D_2(35)$-C_{88}, $Sm_2@C_1(21)$-C_{90}, and $Sm_2@D_3(85)$-C_{92}. All of the structures show some degree of disorder in the position of the fullerene cage and in the positions of the samarium ions on the inside. Details of the disorder are given in the Experimental Section. Solvate toluene molecules are also present for $Sm_2@D_2(35)$-C_{88}, $Sm_2@C_1(21)$-C_{90}, but chlorobenzene is present in $Sm_2@D_3(85)$-C_{92}.

Views of all three new dimetal endohedral isomers in their major occupancy, their relationship to Ni(OEP), and the major Sm positions are displayed in Figures 4, 5 and 6. In these drawings, the solvate molecules are omitted for clarity. The shortest Ni···C distances are shown with a dashed line. These distances

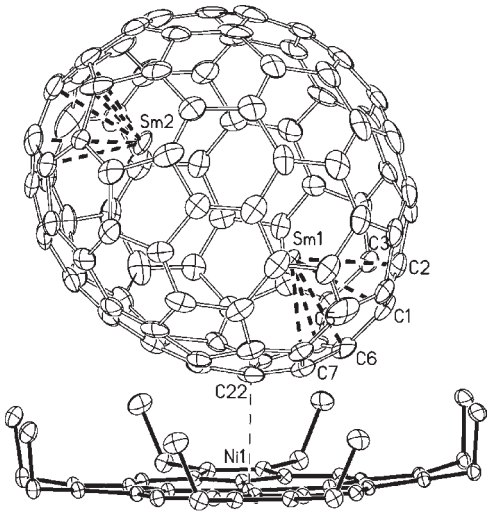

Figure 6. A portion of the structure of $Sm_2@D_2(85)$-C_{92}·Ni(OEP)·2chlorobenzene showing 35% probability displacement ellipsoids for non-hydrogen atoms with the chlorobenzene molecules omitted. The Sm---Sm distance between the major sites with 74% occupancy is 4.6190(6) Å. The range of Sm···C distances is 2.50−2.77 Å.

range from 2.982(4) to 2.989(5) to 2.793(3) Å for $Sm_2@D_2$-(35)-C_{88}·Ni(OEP), $Sm_2@C_1(21)$-C_{90}·Ni(OEP), and $Sm_2@$-$D_3(85)$-C_{92}·Ni(OEP), respectively. The Sm---Sm line subtends an angle with respect to the porphyrin plane of 11.1°, 9.2°, and 39.1°, respectively, which can be compared to the value of 15.4° for $Sm_2@D_{3d}(822)$-C_{104}·Ni(OEP). Both steric and van der Waals effects appear to control how the fullerene is arranged. Specifically, the flatter "waist" regions that are more coronene-like align themselves parallel to the porphyrin plane. This enhances $\pi-\pi$ interactions, but the larger size and steric bulk of the C_{92} cage forces it to tip and utilize more of the "cap" to fit in the porphyrin host. Notably, the latter position leads to a closer Ni···C contact. The six shortest contacts from Sm to carbon are shown with dashed lines. All three fullerenes show short Sm^{2+}···C contacts that have η^6 geometry, although the most symmetrical interaction is seen in the C_{88} cage. In the structure involving the C_{104} cage, the two samarium ions occupy positions near to the 3-fold axis where three hexagons join and do not follow this trend.

The cage isomers all obey the isolated pentagon rule (IPR), which places five hexagons about any pentagon and prohibits pentagon−pentagon contact. The number of possible IPR-obeying isomers increases dramatically as the number of carbon atoms in the fullerene cage increases. Considering only isolated pentagon isomers, the number of possible isomers is 35, 46, and 86 for the C_{88}, C_{90}, and C_{92} cages, respectively.[32] In the case of our previously reported $Sm_2@D_{3d}(822)$-C_{104}, there were 823 possible isomers. None of the structures of these samarium endohedrals involves a carbide, although $Sm_2@D_3(85)$-C_{92} and $Gd_2(\mu\text{-}C_2)$-$@D_3(85)$-C_{92} utilize the same fullerene cage.[9] It also should be pointed out that these three new endohedral fullerenes with cage isomers having D_2, C_1, and D_3 symmetry are chiral, whereas the fullerene is situated at a crystallographic site with mirror symmetry. Thus, a racemate of the endohedral occupies a common crystallographic site in a disordered fashion.

Figure 7 shows how the axes of the fullerene cages are aligned relative to the porphyrin plane. The heavier lines show the principal

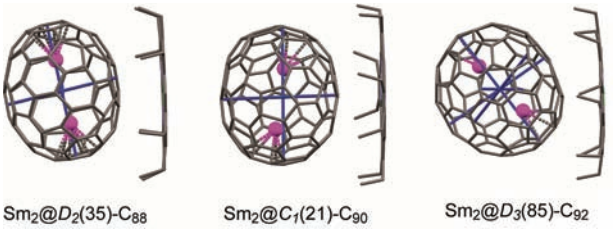

Figure 7. The disposition of the principal symmetry axes of the fullerene with respect to the cocrystallized Ni(OEP).

rotation axes of $Sm_2@D_2(35)$-C_{88}·Ni(OEP) and $Sm_2@D_3(85)$-C_{92}·Ni(OEP) and the major and minor cage axes in $Sm_2@C_1(21)$-C_{90}·Ni(OEP). For $Sm_2@C_1(21)$-C_{90}, the longest and shortest perpendicular axes are shown. In the C_{88} cage, there are three perpendicular 2-fold axes with lengths defined by (1) hexagon ring centroids with a distance of 8.518 Å; (2) 6:6 ring junctions with a distance of 8.915 Å, viewed out of page; and (3) 6:6 ring junctions with a short distance of 7.241 Å, which face the porphyrin. The main samarium site lies along the axis (1) that passes through the hexagons and allows it to have a symmetrical η^6 interaction while still maintaining a long Sm---Sm distance. In the C_{90} cage, there are no axes of symmetry, but the longest dimension is 9.058 Å and corresponds to the distance between two opposing pentagon−hexagon−hexagon junctions (PHJ). There is a short perpendicular distance passing through a hexagon−hexagon−hexagon junction (THJ) of 7.589 Å that faces the porphyrin. The two Sm atoms lie in a line that is tipped by 24.1° from the major axis, allowing them to reside in the position for optimal η^6 interaction with the cage. In the C_{92} cage, the principal 3-fold axis passes through a THJ with a C1···C92 distance of 9.574 Å. Similar to the C_{90} case, the Sm atoms prefer to achieve a long separation while maintaining an η^6 orientation toward the cage and reside to the side of the major axis. There are three perpendicular 2-fold axes with distances computed from 6:6 ring junction centroids. Their mean distance is 8.263 Å with an average deviation from the mean of 0.014 Å.

Figure 8 shows the positions of the samarium atoms inside the three cages as viewed down the shortest cage axis. The occupancies of the various Sm sites are given in the caption. In these three endohedrals, the samarium atoms are arranged in a ring that is perpendicular to the shortest cage axis. However, in $Sm_2@D_{3d}$-(822)-C_{104}, there are only three Sm positions (disorder 0.74/0.17/0.09), very close to the poles of the long axis beneath the canopy of the triple hexagons through which the 3-fold axis passes. Disorder in the positions of the Sm^{2+} ions inside the fullerene cage can be expected to correlate to a Boltzman distribution of sites corresponding to potential energy surfaces with relatively low barriers between minima. In other midsized endohedral fullerenes, $La_2@I_h$-C_{80},[33,34] $Ce_2@I_h$-C_{80},[35] $Er_2@C_s(6)$-C_{82},[10] $Er_2@C_{3v}(8)$-C_{82},[11] and $Sc_2(\mu_2\text{-O})@C_s(6)$-$C_{82}$,[36] the disordered metal sites are found along bands of 10 contiguous hexagons, but such bands are lacking in the $Sm_2@C_{2n}$ endohedrals. In these midsized cages, the two metal cations must coexist without significant bonding at a distance only slightly larger than the sum of their covalent radii. In the smallest characterized dimetalloendohedral fullerenes, $Ce_2@C_{72}$[15] and $La_2@C_{72}$,[37] the IPR cage is simply too crowded, and the stable isomer is a non-IPR cage with two pentalene "noses" that accommodate the metal ions, thus allowing them to be further apart. However, even with only one metal cation, a similar circular array of disordered samarium

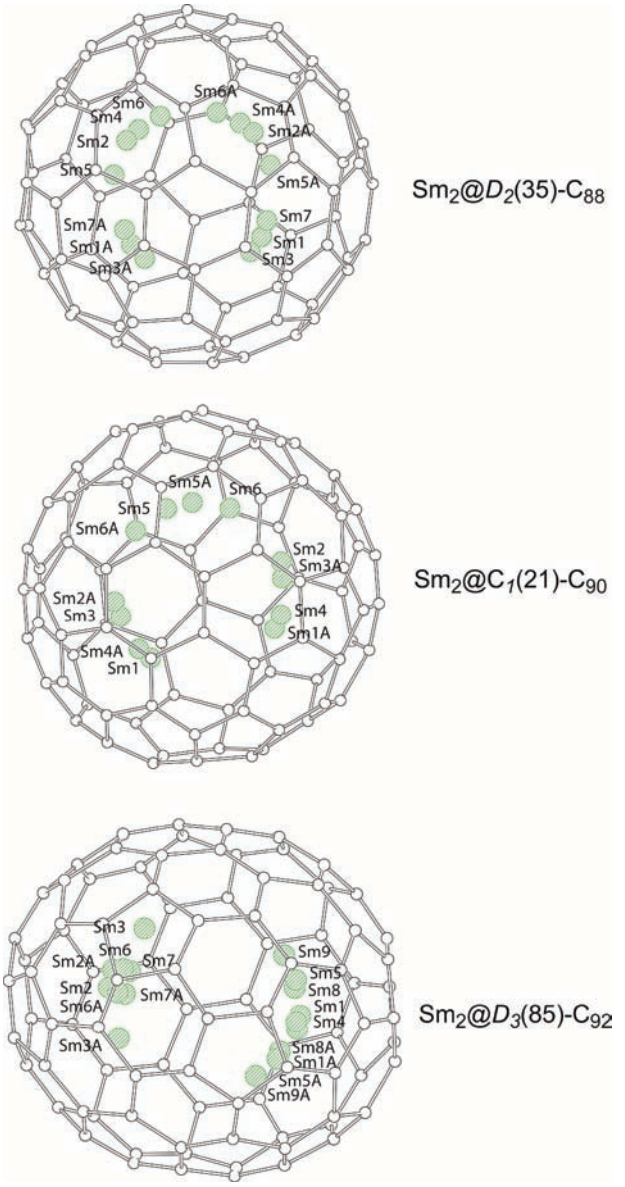

Figure 8. Views looking down the shortest cage dimension showing the distribution of Sm positions. The longest cage dimension is horizontal. Those Sm atoms labeled "A" are generated by the crystallographic mirror plane. Occupancies for $Sm_2@D_2(35)$-C_{88}·Ni(OEP) are: Sm1, 0.27; Sm2, 0.27; Sm3, 0.15; Sm4, 0.15; Sm5, 0.06; Sm6, 0.05; Sm7, 0.05. For $Sm_2@C_1(21)$-C_{90}·Ni(OEP): Sm1, 0.322; Sm2, 0.216; Sm3, 0.146; Sm4, 0.146; Sm5, 0.119; Sm6, 0.051. For $Sm_2@D_2(85)$-C_{92}: Sm1, 0.38; Sm2, 0.38; Sm3, 0.06; Sm4, 0.06; Sm5, 0.05; Sm6, 0.02; Sm7, 0.02; Sm8, 0.015; Sm9, 0.015.

atom positions is seen in the four Sm@C_{90} isomers recently described.[24] In our larger cages ≥C_{88}, where there are two metal cations and no contiguous bands of hexagons, the major site or sites prefer to position the two nonbonded metal ions as distant as possible along the long axis of the cage.

Table 1 shows the cage dimensions for the $Sm_2@C_{2n}$ endohedrals along with the separations between the samarium ions. These data indicate that expansion of the cage size results in increased distances between the samarium ions. This behavior is consistent with repulsive Coulombic interactions between the samarium ions.

Table 1. Cage Dimensions and Samarium Atom Separations

	$Sm_2@D_2(35)$-C_{88}	$Sm_2@C_1(21)$-C_{90}	$Sm_2@D_3(85)$-C_{92}	$Sm_2@D_{3d}(822)$-C_{104}[a]
longest cage dimen(s), Å	8.518, 8.915	9.058	9.574	10.840
shortest cage dimen(s), Å	7.241	7.589	8.247, 8.254, 8.289	8.241, 8.255, 8.296
major Sm---Sm distances, Å	4.216, 4.206	4.147	4.619, 4.604	5.832
range Sm---Sm distances, Å	3.804−4.228	3.824−4.366	4.326−4.648	5.428−5.832

[a] Data from: Mercado, B. Q.; Jiang, A.; Yang, H.; Wang, Z. M.; Jin, H. X.; Liu, Z. Y.; Olmstead, M. M.; Balch, A. L. *Angew. Chem., Int. Ed.* **2009**, *48*, 9114−9116.

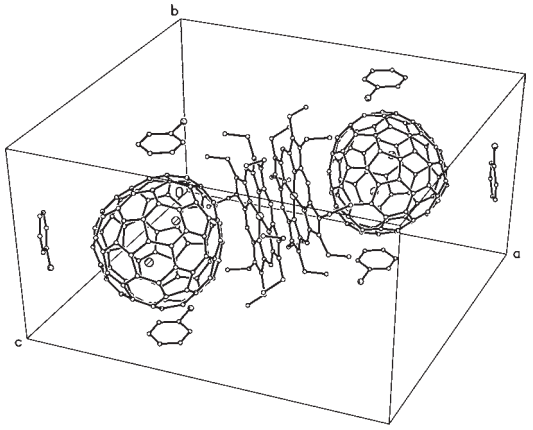

Figure 9. View of the packing of $Sm_2@D_3(85)$-C_{92}·Ni(OEP)·2chlorobenzene.

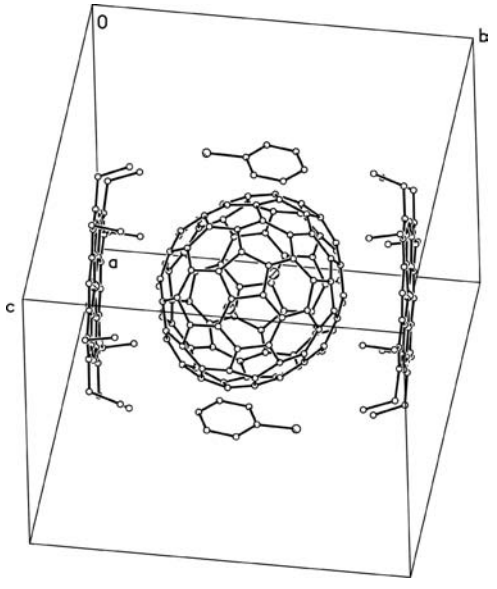

Figure 10. View of the packing of $Sm_2@C_{104}$·2Ni(OEP)·chlorobenzene.

The three new endohedrals crystallize in the monoclinic space group *C*2/*m*. The packing of fullerene, Ni(OEP), and solvate (toluene or chlorobenzene) is similar in all three structures. Figure 9 gives an example of the packing arrangement as found in the structure of $Sm_2@D_3(85)$-C_{92}·Ni(OEP)·2chlorobenzene. There is a back-to-back arrangement of two Ni(OEP) molecules about a center of symmetry, encapsulation of the fullerene in the eight ethyl groups that project outward in the same direction

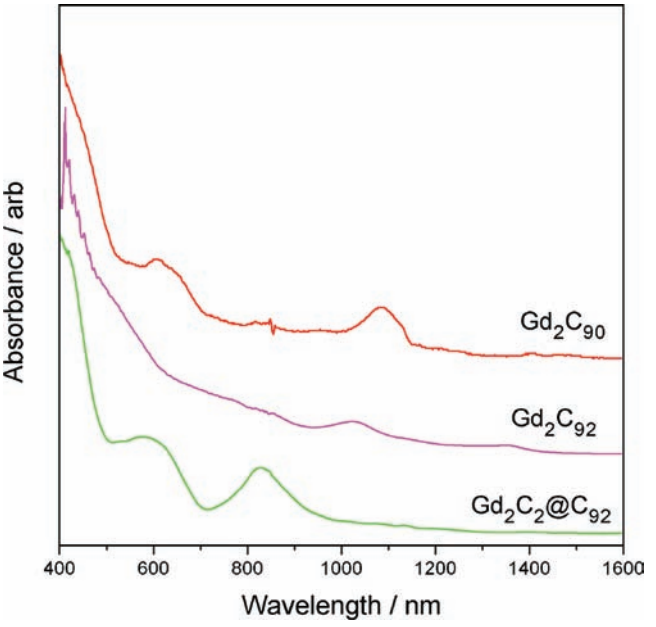

Figure 11. UV/vis/NIR absorption spectra of the isolated Gd_2C_{2n} (n = 44−46) endohedral fullerenes dissolved in carbon disulfide.

from the porphyrin plane, and face-to-ball packing of the aromatic rings of the solvate groups with the fullerene. The stoichiometry of fullerene:porphyrin:aromatic molecule is 1:1:2. The disordered fullerene and the porphyrin are located on crystallographic mirror planes, but the fullerene cage itself does not have mirror symmetry. Only one side of the fullerene shows a close porphyrin contact. The remaining sides are in close contact with chlorobenzene molecules.

As shown in Figure 10, this structural type is not replicated in the crystal structure of $Sm_2@D_{3d}(822)$-C_{104}·2Ni(OEP)·chlorobenzene when it is crystallized under the same conditions. Instead, the crystal system is monoclinic, space group $P2_1/n$, and the fullerene is surrounded by two molecules of Ni(OEP) and has only one chlorobenzene in the formula unit, giving a stoichiometry of 1:2:1. In this case, the fullerene has true crystallographic inversion symmetry.

Spectroscopic Comparison of $Sm_2@C_{2n}$ and Gd_2C_{2n} Endohedral Fullerenes. Figure 11 shows the UV/vis/NIR spectra of Gd_2C_{90}, Gd_2C_{92}, and $Gd_2(\mu\text{-}C_2)@D_3(85)$-$C_{92}$, whose preparations were reported earlier.[9] Their chromatographic behavior and mass spectra are given in the Supporting Information. The UV/vis/NIR spectra of endohedral fullerenes are known to depend upon the cage size and cage isomer found in a particular molecule.[1,2] Thus, $Sm_2@D_3(85)$-C_{92} and $Gd_2(\mu\text{-}C_2)@D_3(85)$-$C_{92}$ are expected to display and indeed do display similar UV/vis/NIR spectra, because they both have been shown crystallographically

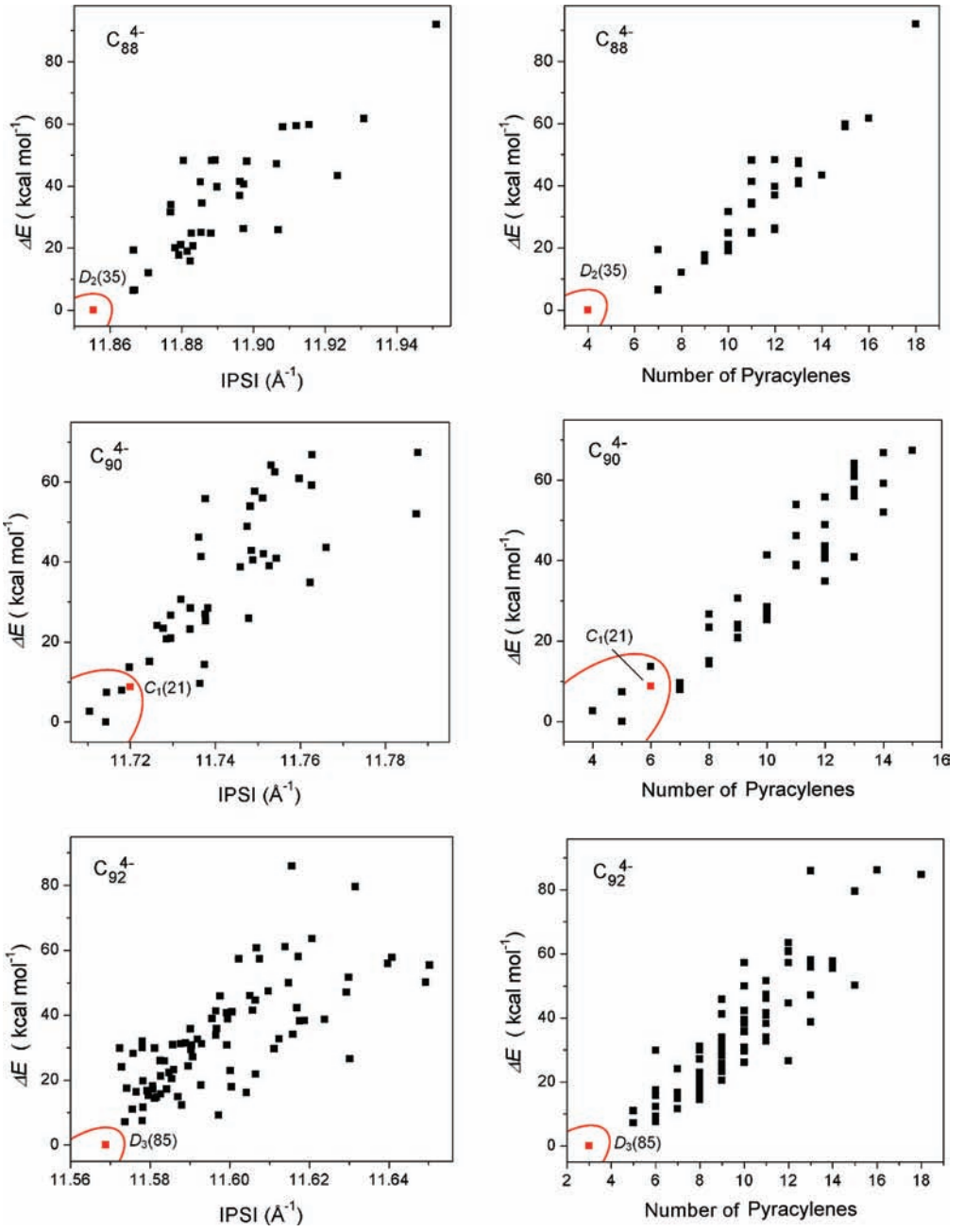

Figure 12. Correlations between relative stability of the fullerene tetra-anions and IPSI as well as the number of pyracylene units in all of the IPR cages of C_{88}, C_{90}, and C_{92}, respectively. The calculations were carried out at the B3LYP/3-21G level. The isomers of metallofullerenes with a red mark were experimentally identified in this work.

to involve the same $D_3(85)$-C_{92} cage. Because the UV/vis/NIR spectra of Gd_2C_{90} and Gd_2C_{92} are nearly identical to those of $Sm_2@D_2(35)$-C_{88} and $Sm_2@C_1(21)$-C_{90}, we suggest that Gd_2C_{90} and Gd_2C_{92} are the carbides $Gd_2(\mu\text{-}C_2)@D_2(35)$-$C_{88}$ and $Gd_2(\mu\text{-}C_2)@C_1(21)$-$C_{90}$, respectively.

Computations Regarding the Stability of the Cage Isomers. Metal containing endohedral fullerenes involve significant electron transfer from the electropositive metal atoms to the carbon cage.[7] In the case of endohedrals containing two samarium atoms, the cage will acquire a 4− charge as a result of the transfer of electrons that produces two Sm^{2+} ions on the inside. Likewise, four electron transfer to the cage is involved in the carbides containing a $\{(Gd^{3+})_2(\mu\text{-}C_2^{2-})\}^{4+}$ unit. Theoretical studies have shown that the most stable isomer for a particular cage size depends upon two factors: the molecular orbital HOMO−LUMO gap for the corresponding anionic empty cage fullerene and the need to maximally separate the pentagons, which are the sites of negative charge in the fulleride anions.[38,39] For C_{88}, C_{90}, and C_{92} with tetra-anionic cages, the computed HOMO−LUMO gap is only large for two of the C_{92} cages, $D_3(85)$-C_{92} (0.86 eV) and $C_1(67)$-C_{92} (0.84 eV), while the gaps for the isomers of C_{88} and C_{90} cages are smaller.[40] Thus, consideration of the HOMO−LUMO gap does not allow a clear prediction of which cage will be favored for the tetra-anions of C_{88} and C_{90}.

Table 2. Crystal Data and Data Collection Parameters

	$Sm_2@D_2(35)$-C_{88} ·Ni(OEP)·2toluene	$Sm_2@C_1(21)$-C_{90} ·Ni(OEP)·2toluene	$Sm_2@D_3(85)$-C_{92} ·Ni(OEP)· 2chlorobenzene
formula	$C_{138}H_{60}N_4NiSm_2$	$C_{140}H_{60}N_4NiSm_2$	$C_{140}H_{54}Cl_2N_4NiSm_2$
fw	2133.31	2157.33	2006.98
color, habit	black, parallelepiped	black, parallelepiped	black, parallelepiped
crystal system	monoclinic	monoclinic	monoclinic
space group	*C*2/*m*	*C*2/*m*	*C*2/*m*
a, Å	25.108(5)	25.4420(13)	25.5870(9)
b, Å	15.372(3)	15.4299(8)	14.9402(6)
c, Å	20.633(4)	20.6732(11)	21.3995(7)
β, deg	94.469(2)	95.291(5)	97.638(2)
V, Å^3	7939(3)	8081.0(7)	8107.9(5)
Z	4	4	4
T, K	120	100	100
radiation (*λ*, Å)	synchrotron, 0.68890	synchrotron, 0.77490	synchrotron 0.77490
unique data	12 105 [*R*(int) = 0.034]	18 152 [*R*(int) = 0.050]	17 327 [*R*(int) = 0.033]
obsd ($I > 2\sigma(I)$) data	10 949	15 318	13 411
R1[a] (obsd data)	0.0604	0.1022	0.0473
wR2[b] (all data)	0.1709	0.3027	0.1412

[a] For data with $I > 2\sigma(I)$, R1 = $(\Sigma||F_O| - |F_C||)/(\Sigma|F_O|)$. [b] For all data, $((\Sigma[w(F_O^2 - F_C^2)])/(\Sigma[w(F_O^2)^2]))^{1/2}$.

Two criteria have been developed to evaluate the separation of the pentagons in a particular fullerene cage isomer.[7] The inverse pentagon separation index (IPSI) (see eq 1 where R_{ij} is the separation between the centers of pentagons) is a simple geometric measure of the separation between pentagons. Additionally, minimization of the number of pyracylene units in a cage isomer structure results in a great pentagon separation.

$$\mathrm{IPSI} = \sum_{i=1}^{12}\sum_{j>i}^{12} 1/R_{ij} \qquad (1)$$

Figure 12 shows the correlations between relative stability of the fullerene tetra-anions and the inverse pentagon separation index (IPSI) and the number of pyracylene units in C_{88}, C_{90}, and C_{92} IPR cages. These two criteria agree that the $D_2(35)$-C_{88} and $D_3(85)$-C_{92} cages are the best hosts for the $\{(Sm^{2+})_2\}^{4+}$ and $\{Gd_2(\mu\text{-}C_2)\}^{4+}$guests, but the situation is less clear for the C_{90} cage. As noted earlier, entropic factors may be significant in determining which cage isomer predominates at the relatively high temperatures used for the formation of these endohedrals.[41,42]

CONCLUSIONS

The three new disamarium endohedrals with IPR-obeying cages have been purified and structurally characterized as $Sm_2@D_2$-(35)-C_{88}, $Sm_2@C_1(21)$-C_{90}, and $Sm_2@D_3(85)$-C_{92}. The cage found in $Sm_2@D_2(35)$-C_{88} has been encountered previously in $Tb_3N@D_2(35)$-C_{88}, the only other endohedral with this cage size that has been characterized by X-ray crystallography.[43] Likewise, $Sm_2@D_3(85)$-C_{92} and $Gd_2(\mu\text{-}C_2)@D_3(85)$-$C_{92}$, the only other endohedrals involving 92 carbon atoms to be crystallographically identified, share a common fullerene cage as noted earlier. In contrast, the carbon cage found in $Sm_2@C_1(21)$-C_{90} has never before been characterized by X-ray diffraction, although the crystal structures of three empty cage isomers of C_{90} ($D_{5h}(1)$-C_{90},[44] $C_1(30)$-C_{90}, and $C_1(32)$-C_{90}[45]) have been reported along with those of four isomers of $Sm@C_{90}$ ($Sm@C_2(40)$-C_{90}, $Sm@C_2(42)$-C_{90}, $Sm@C_{2v}(45)$-C_{90}, and $Sm@C_2(46)$-C_{90}).[24]

Under similar conditions, monosamarium containing endohedrals, $Sm@C_{2n}$, are formed in greater abundance than the disamarium endohedrals, $Sm_2@C_{2n}$, while digadolinium-containing endohedrals dominate over the formation of monogadolinium endohedrals, $Gd@C_{2n}$. However, the structures of the disamarium and digadolinium endohedrals differ. All of the disamarium endohedrals discussed here are normal endohedrals, not carbide containing endohedrals. In contrast, carbide formation appears to dominate in the digadolinium endohedrals, at least for the smallest members of the series: $Gd_2(\mu\text{-}C_2)@D_2(35)$-$C_{88}$, $Gd_2(\mu\text{-}C_2)@C_1(21)$-$C_{90}$, and $Gd_2(\mu\text{-}C_2)@D_3(85)$-$C_{92}$. Nevertheless, for all of the compounds considered here ($Sm_2@D_2(35)$-C_{88}, $Sm_2@C_1(21)$-C_{90}, $Sm_2@D_3(85)$-C_{92}, $Sm_2@D_{3d}(822)$-C_{104}, $Gd_2(\mu\text{-}C_2)@D_2(35)$-$C_{88}$, $Gd_2(\mu\text{-}C_2)@C_1(21)$-$C_{90}$, and $Gd_2(\mu\text{-}C_2)@D_3(85)$-$C_{92}$), the carbon cage bears a 4− charge, while the interior atoms carry a 4+ charge as $\{(Sm^{2+})_2\}^{4+}$ or $\{(Gd^{3+})_2(\mu\text{-}C_2^{2-})\}^{4+}$.

EXPERIMENTAL SECTION

Synthesis of the $Sm_2@C_{2n}$ Endohedrals. A 8 × 150 mm graphite rod filled with Sm_2O_3 and graphite powder (Sm:C atomic ratio 1:40) was vaporized as the anode in DC arc discharge under optimized conditions. The raw soot was sonicated in *o*-dichlorobenzene for 8 h and then filtered with the aid of a vacuum. After the solvent was removed with a rotary evaporator, chlorobenzene was added to redissolve the dry extract. The resulting solution was subjected to a four-stage HPLC isolation process without recycling. Chromatographic details are given in the Supporting Information.

The purity and composition of the samples were verified by laser desorption ionization time-of-flight mass spectrometry (LDI-TOF-MS). Ultraviolet−visible−near-infrared (UV−vis−NIR) spectra were obtained through the use of a UV-3600 spectrophotometer (Shimadzu Corp.) with samples dissolved in carbon disulfide.

Crystal Growth. Co-crystals of the $Sm_2@C_{2n}$ endohedrals and Ni^{II}(OEP) were obtained by layering a nearly saturated solution of the endohedral in toluene or chlorobenzene over a red toluene solution of Ni^{II}(OEP) in a glass tube. Over a 14-day period, the two solutions diffused together and black crystals formed.

Crystal Structure Determinations. Crystal data are given in Table 2. Black crystals of $Sm_2@D_2(35)$-C_{88}·Ni(OEP)·2toluene were mounted in the 120(2) K nitrogen cold stream provided by an Oxford Cryostream low temperature apparatus on the goniometer head of a Rigaku Crystal-Logic Kappa diffractometer equipped with a Saturn 724+ detector, on beamline I19 at the Diamond Light Source Ltd. in Oxfordshire, UK. Diffraction data were collected using synchrotron radiation monochromated with silicon(111) to a wavelength of 0.68890 Å. Black crystals of $Sm_2@C_1(21)$-C_{90}·Ni(OEP)·2toluene and $Sm_2@D_2$-(85)-C_{92}·Ni(OEP)·2chlorobenzene were mounted in the nitrogen cold stream provided by an Oxford Cryostream low temperature apparatus on the goniometer head of a Bruker D8 diffractometer equipped with an ApexII CCD detector at the Advanced Light Source, Berkeley, CA, beamline 11.3.1. Data were collected with the use of silicon(111) monochromated synchrotron radiation (λ = 0.77490 Å). All three data sets were reduced with the use of Bruker SAINT,[46] and a multiscan absorption correction was applied with the use of SADABS.[47] The structures were solved by direct methods (SHELXS97) and refined by full-matrix least-squares on F^2 (SHELXL97).[48]

$Sm_2@D_2(35)$-C_{88}·Ni(OEP)·2toluene. The C_{88} fullerene cage is disordered with respect to a crystallographic mirror plane that bisects the molecule, but is not a symmetry element for the fullerene. Thus, there are two orientations of the C_{88} ball. Because of the crystallographic mirror plane, these two occupancies must sum to 0.5. These orientations were initially refined with variable occupancies and subsequently fixed at the converged values of 0.37 (74%) and 0.13 (26%), respectively. The major orientation was refined with anisotropic displacement parameters. The minor isomer was pasted in, based on the geometry of the major isomer, with the use of the FRAG command and kept fixed in the final cycles of refinement using isotropic displacement parameters.

There are seven different sites for the samarium atom, which were required to sum to occupancy of 1.0000 by the use of free variables and subsequently refined with fixed occupancies. Only the six sites with highest occupancy were refined with anisotropic displacement parameters; the remaining site utilized isotropic displacement parameters.

$Sm_2@C_1(21)$-C_{90}·Ni(OEP)·2toluene. The C_{90} cage is disordered with respect to a crystallographic mirror plane, and there are two orientations of the C_{90} cage. The structure was solved for the major isomer by atom picking, and the second orientation was determined by trial and error fitting of the rigid group calculated from the original C_{90} followed by rigid group refinement. In the major orientation, atoms C38, C56, C57, C60, and C61 reside on the mirror plane; atoms C14, C15, C26, C27, C28, C29, C31---C37, C39---C53, and C62 are disordered with respect to reflection, and the remaining atoms utilize the mirror symmetry. The occupancy of this orientation was initially refined and then fixed at 0.33 total (out of 0.50), or 66%. Atoms C201---C290 comprise the second orientation at 0.17 (or 34%) occupancy. There is the possibility of at least a third orientation, but it was not possible to include it. Distance restraints, as free variables, were applied to atoms of similar geometric positions, according to the nature of the five- and six-membered ring junctions. Also, specific distance restraints were applied to five atom pairs. There are six positions for Sm atoms in the structure, and they were initially refined with fixed thermal parameters and variable occupancy. In the final cycles of refinement, the occupancies were fixed, and the thermal parameters were allowed to become anisotropic.

$Sm_2@D_2(85)$-C_{92}·Ni(OEP)·2chlorobenzene. The fullerene cage is disordered with respect to mirror site symmetry. The refinement utilized only one orientation of the cage. There are two major sites for samarium and seven others at lower occupancy. The occupancies were initially refined and constrained to add to 1.0000 and then fixed.

Computations on the Hollow C_{88}, C_{90}, and C_{92} IPR Cages. The geometries of each of the IPR cages of C_{88}, C_{90}, and C_{92} were optimized using density functional theory at B3LYP/3-21G level, and those of the tetra-anions were also optimized using the same method. The inverse pentagon separation index (IPSI) for each of the tetra-anions was calculated on the basis of the optimized geometries. In addition, the numbers of pyracylene units in these cages were enumerated using a small program written by us.

■ ASSOCIATED CONTENT

Supporting Information. Complete ref 29, and HPLC chromatograms and MS spectra of the purified samples of the three samarium endohedral fullerenes and the two gadolinium endohedral fullerenes. X-ray crystallographic files in CIF format for $Sm_2@D_2(35)$-C_{88}·Ni(OEP)·2toluene, $Sm_2@C_1(21)$-C_{90}·Ni(OEP)·2toluene, and $Sm_2@D_3(85)$-C_{92}·Ni(OEP)·2chlorobenzene. This material is available free of charge via the Internet at http://pubs.acs.org.

■ AUTHOR INFORMATION

Corresponding Author
zyliu@cjlu.edu.cn; mmolmstead@ucdavis.edu; albalch@ucdavis.edu

■ ACKNOWLEDGMENT

We thank the National Science Foundation [Grants CHE-1011760 and CHE-0716843 to A.L.B. and M.M.O.], the National Natural Science Foundation of China [20971108 to Z.L. and 11179039 to H.Y.], and the Natural Science Foundation of Zhejiang Province of China [Y4090430 to Z.W.] for support. We also thank the Diamond Light Source for support, and Dr. Simon Teat and The Advanced Light Source, supported by the Director, Office of Science, Office of Basic Energy Sciences, of the U.S. Department of Energy under contract no. DE-AC02-05CH11231, for beam time.

■ REFERENCES

(1) Akasaka, T.; Nagase, S. *Endofullerenes: A New Family of Carbon Clusters*; Kluwer Academic Publishers: Dordrecht, The Netherlands, 2002.

(2) Akasaka, T., Wudl, F., Nagase, S., Eds. *Chemistry of Nanocarbons*; John Wiley & Sons, Ltd.: Singapore, 2010.

(3) Mikawa, M.; Kato, H.; Okumura, M.; Narazaki, M.; Kanazawa, Y.; Miwa, N.; Shinohara, H. *Bioconjugate Chem.* **2001**, *12*, 510–514.

(4) Bolskar, R. D.; Benedetto, A. F.; Husebo, L. O.; Price, R. E.; Jackson, E. F.; Wallace, S.; Wilson, L. J.; Alford, J. M. *J. Am. Chem. Soc.* **2003**, *125*, 5471–5478.

(5) Caravan, P.; Ellison, J. J.; McMurry, T. J.; Lauffer, R. B. *Chem. Rev.* **1999**, *99*, 2293–2352.

(6) Iezzi, E. B.; Duchamp, J. C.; Fletcher, K. R.; Glass, T. E.; Dorn, H. C. *Nano Lett.* **2002**, *2*, 1187–1190.

(7) Rodríguez-Fortea, A.; Balch, A. L.; Poblet, J. M. *Chem. Soc. Rev.* **2011**, *40*, 3551–3563.

(8) Lu, X.; Akasaka, T.; Nagase, S. *Chem. Commun.* **2011**, *47*, 5942–5957.

(9) Yang, H.; Lu, C.; Liu, Z.; Jin, H.; Che, Y.; Olmstead, M. M.; Balch, A. L. *J. Am. Chem. Soc.* **2008**, *130*, 17296–17300.

(10) Olmstead, M. M.; de Bettencourt-Dias, A.; Stevenson, S.; Dorn, H. C.; Balch, A. L. *J. Am. Chem. Soc.* **2002**, *124*, 4172–4173.

(11) Olmstead, M. M.; Lee, H. M.; Stevenson, S.; Dorn, H. C.; Balch, A. L. *Chem. Commun.* **2002**, 2688–2689.

(12) (a) Akasaka, T.; Nagase, S.; Kobayashi, K.; Walchli, M.; Yamamoto, K.; Funasaka, H.; Kako, M.; Hoshino, T.; Erata, T. *Angew. Chem., Int. Ed.* **1997**, *36*, 1643–1645. (b) Yamada, M.; Wakahara, T.; Nakahodo, T.; Tsuchiya, T.; Maeda, Y.; Akasaka, T.; Yoza, K.; Horn, E.; Mizorogi, N.; Nagase, S. *J. Am. Chem. Soc.* **2006**, *128*, 1402–1403. (c) Wakahara, T.; Yamada, M.; Takahashi, S.; Nakahodo, T.; Tsuchiya, T.; Maeda, Y.; Akasaka, T.; Kako, M.; Yoza, K.; Horn, E.; Mizorogi, N.;

Nagase, S. *Chem. Commun.* **2007**, 2680–2682. (d) Yamada, M.; Someya, C.; Wakahara, T.; Tsuchiya, T.; Maeda, Y.; Akasaka, T.; Yoza, K.; Horn, E.; Liu, M. T. H.; Mizorogi, N.; Nagase, S. *J. Am. Chem. Soc.* **2008**, *130*, 1171–1176.

(13) (a) Cao, B. P.; Wakahara, T.; Tsuchiya, T.; Kondo, M.; Maeda, Y.; Rahman, G. M. A.; Akasaka, T.; Kobayashi, K.; Nagase, S.; Yamamoto, K. *J. Am. Chem. Soc.* **2004**, *126*, 9164–9165. (b) Yamada, M.; Wakahara, T.; Tsuchiya, T.; Maeda, Y.; Kako, M.; Akasaka, T.; Yoza, K.; Horn, E.; Mizorogi, N.; Nagase, S. *Chem. Commun.* **2008**, 558–560.

(14) Cao, B.; Nikawa, H.; Nakahodo, T.; Tsuchiya, T.; Maeda, Y.; Akasaka, T.; Sawa, H.; Slanina, Z.; Mizorogi, N.; Nagase, N. *J. Am. Chem. Soc.* **2008**, *130*, 983–989.

(15) Lu, X.; Nikawa, H.; Nakahodo, T.; Tsuchiya, T.; Ishitsuka, M. O.; Maeda, Y.; Akasaka, T.; Toki, M.; Sawa, H.; Slanina, Z.; Mizorogi, N.; Nagase, S. *J. Am. Chem. Soc.* **2008**, *130*, 9129–9136.

(16) Yamada, M.; Wakahara, T.; Tsuchiya, T.; Maeda, Y.; Akasaka, T.; Mizorogi, N.; Nagase, S. *J. Phys. Chem. A* **2008**, *112*, 7627–7631.

(17) Lu, X.; Nikawa, H.; Tsuchiya, T.; Maeda, Y.; Ishitsuka, M. O.; Akasaka, T.; Toki, M.; Sawa, H.; Slanina, Z.; Mizorogi, N.; Nagase, S. *Angew. Chem., Int. Ed.* **2008**, *47*, 8642–8645.

(18) Shi, Z. Q.; Wu, X.; Wang, C. R.; Lu, X.; Shinohara, H. *Angew. Chem., Int. Ed.* **2006**, *45*, 2107–2111.

(19) Kurihara, H.; Lu, X.; Iiduka, Y.; Mizorogi, N.; Slanina, Z.; Tsuchiya, T.; Akasaka, T.; Nagase, S. *J. Am. Chem. Soc.* **2011**, *133*, 2382–2385.

(20) Inoue, T.; Tomiyama, T.; Sugai, T.; Okazaki, T.; Suematsu, T.; Fujii, N.; Utsumi, H.; Nojima, K.; Shinohara, H. *J. Phys. Chem. B* **2004**, *108*, 7573–7579.

(21) Mercado, B. Q.; Jiang, A.; Yang, H.; Wang, Z. M.; Jin, H. X.; Liu, Z. Y.; Olmstead, M. M.; Balch, A. L. *Angew. Chem., Int. Ed.* **2009**, *48*, 9114–9116.

(22) Huang, H.; Yang, S. *J. Phys. Chem. B* **1998**, *102*, 10196–10200.

(23) Okazaki, T.; Lian, Y.; Gu, Z.; Suenaga, K.; Shinohara, H. *Chem. Phys. Lett.* **2000**, *320*, 435–440.

(24) Liu, J.; Shi, Z. J.; Gu, Z. N. *Chem.-Asian J.* **2009**, *4*, 1703–1711.

(25) Lian, Y.; Shi, Z.; Zhou, X.; He, X.; Gu, Z. *Chem. Mater.* **2001**, *13*, 39–42.

(26) Okazaki, T.; Suenaga, K.; Lian, Y.; Gu, Z.; Shinohara, H. *J. Chem. Phys.* **2000**, *113*, 9593–9597.

(27) Yang, H.; Jin, H. X.; Zhen, H.; Wang, Z. M.; Liu, Z. L.; Beavers, C. M.; Mercado, B. Q.; Olmstead, M. M.; Balch, A. L. *J. Am. Chem. Soc.* **2011**, *133*, 6299–6306.

(28) Bolskar, R. D.; Benedetto, A. F.; Husebo, L. O.; Price, R. E.; Jackson, E. F.; Wallace, S.; Wilson, L. J.; Alford, M. J. *J. Am. Chem. Soc.* **2003**, *125*, 5471–5478.

(29) Akasaka, T.; et al. *J. Am. Chem. Soc.* **2008**, *130*, 12840–12841.

(30) Raebiger, J. W.; Bolskar, R. D. *J. Phys. Chem. C* **2008**, *112*, 6605–6612.

(31) Olmstead, M. M.; Costa, D. A.; Maitra, K.; Noll, B. C.; Phillips, S. L.; Van Calcar, P. M.; Balch, A. L. *J. Am. Chem. Soc.* **1999**, *121*, 7090–7097.

(32) Fowler, P. W.; Manolopoulous, D. E. *An Atlas of Fullerenes*; Clarendon: Oxford, 1995.

(33) Akasaka, T.; Nagase, S.; Kobayashi, K.; Walchli, M.; Yamamoto, K.; Funasaka, H.; Kako, M.; Hoshino, T.; Erata, T. *Angew. Chem., Int. Ed. Engl.* **1997**, *36*, 1643–1645.

(34) Nagase, S.; Kobayashi, K.; Akasaka, T. *J. Comput. Chem.* **1998**, *19*, 232–239.

(35) Yamada, M.; Akasaka, T.; Nagase, S. *Acc. Chem. Res.* **2010**, *43*, 92–102.

(36) Mercado, B. Q.; Stuart, M. A.; Mackey, M. A.; Pickens, J. E.; Confait, B. S.; Stevenson, S.; Easterling, M. L.; Valencia, R.; Rodriguez-Fortea, A.; Poblet, J. M.; Olmstead, M. M.; Balch, A. L. *J. Am. Chem. Soc.* **2010**, *132*, 12098–12105.

(37) Kato, H.; Taninaka, A.; Sugai, T.; Shinohara, H. *J. Am. Chem. Soc.* **2003**, *125*, 7782–7783.

(38) Campanera, J. M.; Bo, C.; Poblet, J. M. *Angew. Chem., Int. Ed.* **2005**, *44*, 7230–7233.

(39) Rodriguez-Fortea, A.; Alegret, N.; Balch, A. L.; Poblet, J. M. *Nature Chem.* **2010**, *2*, 955–961.

(40) Valencia, R.; Rodriguez-Fortea, A.; Poblet, J. M. *J. Phys. Chem. A* **2008**, *112*, 4550–4555.

(41) Mercado, B. Q.; Stuart, M. A.; Mackey, M. A.; Pickens, J. E.; Confait, B. S.; Stevenson, S.; Easterling, M. L.; Valencia, R.; Rodriguez-Fortea, A.; Poblet, J. M.; Olmstead, M. M.; Balch, A. L. *J. Am. Chem. Soc.* **2010**, *132*, 12098–12105.

(42) Mercado, B. Q.; Chen, N.; Rodriguez-Fortea, A.; Mackey, M. A.; Stevenson, S.; Echegoyen, L.; Poblet, J. M.; Olmstead, M. M.; Balch, A. L. *J. Am. Chem. Soc.* **2011**, *133*, 6752–6760.

(43) Zuo, T.; Beavers, C. M.; Duchamp, J. C.; Campbell, A.; Dorn, H. C.; Olmstead, M. M.; Balch, A. L. *J. Am. Chem. Soc.* **2007**, *129*, 2035–2043.

(44) Yang, H.; Beavers, C. M.; Wang, Z.; Jiang, A.; Liu, Z.; Jin, H.; Mercado, B. Q.; Olmstead, M. M.; Balch, A. L. *Angew. Chem., Int. Ed.* **2010**, *49*, 886–890.

(45) Yang, H.; Mercado, B. Q.; Jin, H.; Wang, Z.; Jiang, A.; Liu, Z.; Beavers, C.; Olmstead, M. M.; Balch, A. L. *Chem. Commun.* **2011**, *47*, 2068–2070.

(46) *Bruker SAINT*; Bruker AXS Inc.: Madison, WI, 2009.

(47) Sheldrick, G. M. *SADABS*; University of Göttingen: Germany, 2008.

(48) Sheldrick, G. M. *Acta Crystallogr.* **2008**, *A64*, 112–122.